

# Massive quantum superpositions using magneto-mechanics

Sarath Raman Nair,<sup>1,2,\*</sup> Shilu Tian,<sup>3,†</sup> Gavin K. Brennen,<sup>1,2</sup> Sougato Bose,<sup>4</sup> and Jason Twamley<sup>3,‡</sup>

<sup>1</sup>*School of Mathematical and Physical Sciences, Macquarie University, NSW 2109, Australia*

<sup>2</sup>*ARC Centre of Excellence for Engineered Quantum Systems (EQUS), Macquarie University, NSW 2109, Australia*

<sup>3</sup>*Quantum Machines Unit, Okinawa Institute of Science and Technology Graduate University, Onna, Okinawa 904-0495, Japan*

<sup>4</sup>*Department of Physics and Astronomy, University College London, Gower Street, WC1E 6BT London, UK*

Macroscopic quantum superpositions of massive objects are deeply interesting as they have a number of potential applications ranging from the exploration of the interaction of gravity with quantum mechanics to quantum sensing, quantum simulation, and computation. In this letter, we propose two related schemes to prepare a spatial superposition of massive quantum oscillator systems with high Q-factor via a superposition of magnetic forces. In the first method, we propose a large spatial superposition of a levitated spherical magnet generated via magnetic forces applied by adjacent flux qubits. We find that in this method the spatial superposition extent ( $\Delta z$ ) is independent of the size of the particle. In the second method, we propose a large spatial superposition of a magnetically levitated (using the Meissner effect) flux qubit, generated via driving the levitated qubit inductively. In both schemes, we show that ultra-large superpositions  $\Delta z / \delta z_{zpm} \sim 10^6$ , are possible, where  $\delta z_{zpm}$  is the zero point motional extent.

The generation of macroscopic quantum superpositions states, sometimes known as Schrodinger Cat states [1], is one of the most sought-after goals in quantum mechanics. Such superpositions can probe the fundamentals of quantum mechanics and probe the validity of various collapse models [2–6]. By preparing multiple macroscopic quantum superposition states one can test the ability of space-time itself to exist in a quantum superposition state [7–10], and this topic has attracted much attention and discussion recently [10–20]. On the other hand, the generation of a macroscopic quantum superposition is extremely challenging and researchers have proposed a variety of methods for their generation including using supra-molecular complexes [21, 22], using optomechanical systems [23–37], using magneto-mechanical systems [8, 38–42], and cold atomic systems [43, 44]. Recent experimental work in reference [45] shown the demonstration of a macroscopic superposition of bulk acoustic mode of matter which has an effective mass of  $M \sim 16 \mu\text{g}$  [45]. However, the generation of spatial superpositions of the centre of mass of a massive object remains challenging mainly due to the lack of protocols that are capable of achieving large spatial separations of the superpositions for large masses in a robust fashion. In the present work, we describe two complementary levitated setups that have the potential to generate ultra-large spatial superpositions for very massive objects.

In the case of superpositions for large masses, it would be highly desirable to be able to generate a macroscopic Schrodinger cat whose spatial extent is somewhat independent of the mass of the trapped object. To achieve this we must be able to apply a superposition of forces on the trapped object where the magnitude of the force must scale with the mass of the object, i.e. *the force must be intensive*. For this reason, we chose the forces to generate the spatial superpositions based on magnetic actuation. To be specific, we rely on the magnetic forces exerted by superconducting flux qubits

in the present study. Very briefly, in the first method, we describe the generation of spatial superposition on a levitated magnetic sphere using fixed flux qubits situated nearby it, and in the second method, we reverse the first scheme and describe the same on an isolated floating flux qubit levitated by a fixed magnetic sphere. We explain both schemes in detail below.

*General model* – In a general framework we can describe both our schemes as the creation of superposition on a massive quantum harmonic oscillator. For this, we consider a three-dimensional quantum harmonic oscillator (a levitated spherical magnet or a levitated flux qubit) with a mass denoted as  $m$  and which is susceptible to external magnetic actuation. We assume a coordinate system with the origin at this equilibrium position of the oscillator and consider one of the axes, which we denote as  $z$ -axis. We denote the oscillation frequency along this axis as  $\omega_z$ . We consider that this oscillator is in its motional ground state [38, 46], with a ground state width (denoted as  $\delta z_{zpm}$ ),  $\delta z_{zpm} = \sqrt{\hbar/(2M\omega_z)}$ , where  $\hbar$  is the reduced Planck's constant. For the creation of superposition states, we consider logical states  $|0\rangle$  and  $|1\rangle$  based on superconducting flux qubits.

We consider superconducting flux qubit that is made from type-I superconductor (Aluminium). We assume that the operating temperatures for our schemes are at 300 mK or lower and that the magnetic field at the location of the flux qubit is well below its critical magnetic field strength of 9.78 mT to be in the superconducting state [47]. The superconducting flux qubit only allows integer numbers of magnetic flux quantum ( $\Phi_0 = h/2e = 2.068 \times 10^{-15}$  Wb) threading the qubit loop and the flux qubit will generate a supercurrent to compensate any non-integer flux quanta threading through its loop. We assume the superposition currents in the flux qubit to be  $I = \pm 1 \mu\text{A}$  for simplicity in our model. This current can be estimated based on magnetic flux threading the qubit loop as  $p\Phi_0 = \mu_0 I \pi R/2$ , where  $p$  is a dimensionless number defining whether the magnetic flux quanta threading through the loop is an integer or not,  $\mu_0$  and  $R$  are vacuum permeability and the Radius of the flux qubits in our schemes.

Since flux qubits' logical states are determined by the direction of large circulating persistent currents in a superconduct-

\* Joint first authors; Corresponding author : sarath.raman-nair@mq.edu.au

† Joint first authors

‡ Corresponding author : jason.twamley@oist.jp

ing ring (currents flow either clockwise or counterclockwise) [46, 48], the flux qubit can generate logical state-dependent magnetic forces. We denote these logical state-dependent magnetic forces generated by flux qubit as  $\vec{F}_{\text{FQ}}^{(q)}$ , where  $|q\rangle$  is the logical state. In general,  $\vec{F}_{\text{FQ}}^{(q)}$  due to the logical states  $|0\rangle$  and  $|1\rangle$  are in opposite directions and we consider they are along  $+\hat{z}$  and  $-\hat{z}$  respectively. This force displaces the equilibrium position of the oscillator away from  $z = 0$ , to the new position  $z = z_{\text{eq}}$  ( $z = -z_{\text{eq}}$ ), for  $|0\rangle$  ( $|1\rangle$ ) state. However, a restoring force along the  $z$ -axis which can be expressed as  $\vec{F}_{\text{TR}} = -\hat{z}m\omega_z^2 z$  acts on the displaced oscillator that pulls the oscillator back from either  $\hat{z}$  directions towards  $z = 0$ . As a result the oscillator reaches new equilibrium position where  $\vec{F}_{\text{FQ}}^{(q)} + \vec{F}_{\text{TR}} = 0$ . When the qubits are put into the superposition state  $\sim (|0\rangle + |1\rangle)$ , the oscillator is pushed to a macroscopic spatial superposition of spatial extent  $\Delta z = 2z_{\text{eq}}$ . We express the spatial extent in terms of a dimensionless factor defined as  $\chi = \Delta z / \delta z_{\text{zpm}}$ .

The generation of macroscopic quantum superposition is possible if the oscillator stays close to its motional ground state. However, the coherent oscillation of the oscillator in its motional ground state will cease after a finite amount of time due to its undesired interaction with the surroundings [49]. We can consider the  $Q$ -factor of the oscillator which is the ratio of oscillation frequency to the damping rate and its value is determined by the dominating damping mechanism. The larger the motional  $Q$ -factor the longer it will remain close to this ground state with a spatial extent of  $\delta z_{\text{zpm}}$  [50]. We consider that the main source of damping on the oscillator is due to the collisions of gas molecules surrounding the oscillator and assume that the average velocity of the oscillator is much smaller than the velocity of the surrounding gas molecules as in the experiment reported in [51]. Thus the  $Q$  factor of the oscillation for the two types of oscillators we are considering can be generally written as [51, 52],  $Q \approx (\pi \rho r \omega_z / (6P_g)) \times \sqrt{(3k_B T) / M_g}$ , where  $P_g$  is the pressure of the gas,  $k_B$  is the Boltzmann's constant,  $T$  is the temperature at which the experiments are performed,  $M_g$  is the mass of the gas molecule,  $\rho$  is the density of the oscillator and  $r$  is the radius (cross-sectional radius) for a spherical (toroid shaped) oscillator (see [SM]). To estimate this  $Q$ -factor we assume that the gas surrounding the oscillator is Helium [51].

*Motional superposition of a levitated spherical magnet* – In this scheme, we consider a spherical magnet (for example Yttrium Iron Garnet (YIG) magnetic micro-particle), held in a three-dimensional trap as shown in Fig. 1) as the quantum oscillator. The three-dimensional trapping of such a spherical magnet can be experimentally realised either via magnetic levitation [51, 53] or via optical levitation.

We consider the primary axis for the optical trapping is along the  $x$ -axis, which is defined using the axes depicted in Fig. 1. The trapping force is strongest along the  $x$ -axis and weakest along the  $y$ - and  $z$ - axes. We consider the magnetic moment of the YIG micro-sphere, which we denote as  $\vec{m}_0$  is directed along  $+\hat{z}$  in Fig. 1, similar to the experimental study in [51] with a different type of spherical magnet. This can be also arranged using an asymmetric optical trap

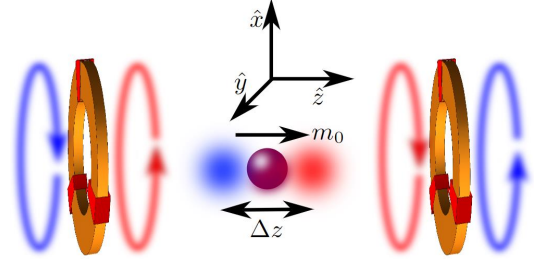


FIG. 1. Schematic for the creation of superposition states of a levitated magnetic YIG micro-particle (oscillator) using superconducting flux qubits (not in scale). We depict the oscillator as a sphere that is trapped at the centre. The nearby flux qubits are shown as rings (orange), containing three Josephson junctions. The two flux qubits are connected to make sure that the supercurrent in each qubit has the same magnitude but opposite circulating directions. When both qubits are in the  $|0\rangle$  ( $|1\rangle$ ) state,  $I$  flows in opposite circularities depicted in red (blue) blurred ring arrows, and the corresponding magnetic field is in anti-Helmholtz configuration. Then qubit state  $|0\rangle|0\rangle$  ( $|1\rangle|1\rangle$ ) shifts to the right (left) by a small distance  $z_{\text{eq}}$  as shown by the red (blue) blurred sphere. By exciting the flux qubits into a superposition state  $\sim (|0\rangle|0\rangle + |1\rangle|1\rangle)$ , the micro-particle is driven into a spatial superposition of extent  $\Delta z = 2z_{\text{eq}}$ .

and asymmetric micro-particle as well. The asymmetric trap will yield motional modes which are highly differentiated in frequency avoiding cross-mode coupling and allows us to manipulate the  $z$ - motional mode specifically. We approximate the YIG sphere as a magnetic dipole due to the spherical shape of the YIG particle. Thus we can write the dipole moment as  $\vec{m}_0 = \mu_0^{-1} B_r V \hat{z}$ , where  $B_r$  is the remnant magnetic field. Furthermore, we consider a pair of flux qubits that is driven and connected such that identical supercurrents which we denote as  $I$  flow with opposite helicity in each qubit. The flux qubit loops are arranged as shown in Fig. 1, and are placed co-axial with the  $z$ -axis symmetrically on either side of the trapped YIG particle. We assume that any change in the magnetic field produced by this YIG at the locations of the flux qubit due to the movement of the YIG within the trap is negligible or compensated appropriately in the experimental implementation.

We model the two flux qubits as superconducting ring with a radius  $R$  [SM]. The flux qubits have supercurrents  $I$  circulating in each ring. The supercurrents generate magnetic fields emanating from each flux qubit such that when each qubit is in the  $|0\rangle$  state, these magnetic fields oppose each other and the magnetic field at the midpoint between the two flux qubits vanishes and varies linearly around there,  $B_z(z) \propto z$ . This magnetic field arrangement corresponds to an anti-Helmholtz configuration. When the flux qubits are flipped to be in the  $|1\rangle$  state the magnetic field at the mid-point again vanishes, it is still in an anti-Helmholtz configuration, but with the linear dependence on  $z$  reversed, e.g.  $B_z(z) \propto -z$ . Thus we can generate a logic state-dependent magnetic field gradient,  $(\partial \vec{B}_z / \partial z)_{|q\rangle}$ , which gives  $\vec{F}_{\text{FQ}}^{(q)} = \vec{m}_0 \cdot (\partial \vec{B}_z / \partial z)_{|q\rangle}$ .

We find that the non-vanishing magnetic field gradient at the origin is maximum when each of these flux qubits is symmetrically located at a distance  $z_{\pm}^{\text{FQ}} = \pm R/2$ , along the  $z$ -axis around the origin [SM] and thus we consider this as the

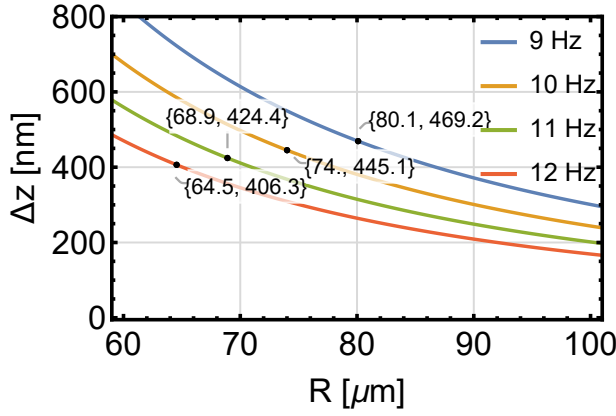


FIG. 2. Numerical analyses of spatial superposition separation,  $\Delta z$  as a function of the radius of flux qubit,  $R$ , for trapping frequency  $\omega_z/(2\pi)$  as shown in the legends, based on equation (1). The markers on each curve represent the  $\{R, \Delta z\}$  values where  $\chi \sim 10^6$  for a YIG sphere with a radius of  $25 \mu\text{m}$ . Please see the main text for more details.

location of the flux qubits for the present scheme. Then the spatial extent of the superposition can be obtained by solving the equation [SM],

$$\frac{3IB_r R^2}{\rho\omega_z^2} \left[ \frac{((\Delta z/2) - (R/2))}{((\Delta z/2) - (R/2))^2 + R^2} - \frac{((\Delta z/2) + (R/2))}{((\Delta z/2) + (R/2))^2 + R^2} \right] + (\Delta z/2) = 0, \quad (1)$$

Counter-intuitively, from equation 1, we can see that  $\Delta z$  is independent of the size of the magnetic sphere but depends only on the magnet's density and remnant magnetization.

We now numerically study the extent of spatial superposition of the YIG sphere in the considered scheme and the results are shown in Fig. 2. In Fig. 2 (a) we show how the spatial superposition extent  $\Delta z$  changes as a function of changing the radius of the flux qubits. We evaluate this numerically from Eq. (1). The numerical values of parameters used for the numerical estimations are given in the supplementary material.

If the levitation of the spherical magnet is via optical means one has to be careful about laser-induced heating of the flux qubit. In order to avoid any direct exposure of the light required for the optical trapping irradiating the flux qubits the latter should be located outside the optical beam path [SM]. One has to be also careful about the optical power required for the trapping considering the low cooling power of dilution refrigeration at mK temperatures. In the case of magnetic levitation of the YIG sphere, we work in the regime where the magnetic field produced by the flux qubits does not affect the levitation mechanism. From Fig. 2 (a) we can see that for the present scheme we can achieve superposition separation  $\Delta z$  of the order of a hundreds of nanometers and it is independent of the size of the microparticle. The trapping of spherical magnets (not YIG) of radius of around  $23.2 \mu\text{m}$  and of around  $25 \mu\text{m}$  have been experimentally demonstrated via magnetic levitation in references [53] and [51] respectively. For the present scheme, we can achieve the  $\chi$  of the order of  $10^6$  [SM] with

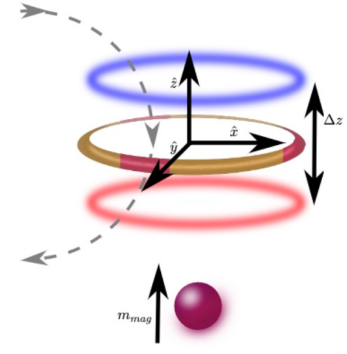


FIG. 3. Schematic for the creation of macroscopic superposition using the levitated superconducting flux qubit (not in scale). The superconducting flux qubit is stably levitated above a spherical micro-magnet due to flux-threading conservation and the Meissner effect. The levitated flux qubit is driven inductively using a nearby superconducting circuit (not shown here) Levitated flux qubit in  $|0\rangle$  ( $|1\rangle$ ) state displaced upward (downward) as depicted by the blue (red) ring. By creating a superposition state of  $|0\rangle$  and  $|1\rangle$  states, the levitated flux qubit is driven into a spatial superposition of extent  $\Delta z = 2z_{eq}$

a spherical magnet (YIG) with a radius  $25 \mu\text{m}$ . For a YIG sphere with radius  $25 \mu\text{m}$ , within the frequency range considered in Fig. 2 we estimate  $Q \sim 10^8$ , due to the damping induced by the surrounding gas collisions on the sphere.

*Motional superposition of a trapped superconducting flux qubit* – We now consider a complementary scheme with an isolated superconducting flux qubit as the oscillator, which itself is magnetically levitated above a spherical magnet as shown schematically in Fig. 3. As we show in the supplementary material [SM], the Q-factor for the oscillator in this scheme can be of the order of  $10^7$ .

We first consider a ring-shaped superconducting flux qubit which is cooled down to the Meissner state via the zero-field cooling method [54]. When the flux qubit is moved above a magnet sphere with a magnet moment  $m_{mag}$ , current will be induced in the qubit to conserve the threading flux, and the flux qubit will feel a repulsive force. Thus the flux qubit can be stably levitated above the magnet at a height  $h$  when we have the flux qubit with proper size (see [SM] for more details on the levitation). We consider an additional superconducting driver circuit situated nearby the flux qubit without any direct galvanic contact to drive the flux qubit. The supercurrent in this driver circuit can generate a magnetic field to change the magnetic flux threading the flux qubit. When the magnetic flux is close to half integer of the flux quantum  $\Phi_0$ , clockwise and anti-clockwise currents will be induced in the flux qubit to compensate for the flux of half flux quantum. So we can inductively drive the flux qubit into the current superposition of  $|0\rangle$  or  $|1\rangle$  states. We denote the modulus of the supercurrent as  $I$ . The flux qubit acquires a resultant qubit state-dependent dipole moment  $\vec{m}_{|q\rangle} = (-1)^q \vec{m}$  (where  $\vec{m} = \hat{z} I \pi R^2$ ) which points downward (upward) when it is  $|0\rangle$  ( $|1\rangle$ ) state. We can then write  $\vec{F}_Q$  for this scheme using the dipole model as,  $\vec{F}_Q^{(q)} = \vec{m}_{|q\rangle} \cdot (\partial \vec{B}_z / \partial z)$ , where  $\vec{B}_z / \partial z$  is the gradient of the magnetic field generated by the fixed spherical magnet. We find  $\vec{F}^{(0)} = \hat{z} 3\mu_0 m_{mag} I R^2 / (2(z+h)^4)$  and

$\vec{F}^{[1]} = -\hat{z}3\mu_0 m_{mag} IR^2 / (2(z+h)^4)$ , where  $z$  is the displacement from the equilibrium height. For  $\Delta z \ll h$ , the spatial position extent is obtained analytically as,

$$\Delta z \sim \frac{3\mu_0 m_{mag} IR^2}{2r^2 \rho \omega_z^2 h^4}. \quad (2)$$

From equation (2), we can see that the spatial superposition can be increased by increasing  $R$  and decreasing both  $\omega_z$  and  $h$ . The equilibrium levitation height  $h$  can be decreased by either reducing the magnetic moment of the magnetic sphere (e.g. by decreasing its radius) or using a higher-density material for the levitated flux qubit. However, to obtain realistic values for this parameter, one needs to analyze the magnetic trapping of the flux qubit above the spherical magnet in detail. When there is no inductive driving, we can approximate the scheme as a levitation of a superconducting ring using a point dipole, due to the spherical nature of the lifting. This problem has been studied analytically in reference [54], but the model does not capture the significant back-action of the superconductor on the magnetic fields that trap it by the Meissner expulsion. Due to the complexity of the problem, a complete analytical solution of the scheme including this backaction is beyond the scope of this present letter. However, to illustrate the effect of back action and how this can be studied analytically we consider a simpler example setup: the Meissner trapping of an SC sphere by two nearby homogenous magnetic spheres (which we consider as magnetic dipoles), arranged in an anti-Helmholtz configuration (see [SM] for more details). We derive an analytical solution for the trap properties along the trapping axis using an exact method not shown before in the literature, to the best of our knowledge, and find that the key parameter, the vertical trap stiffness is modified by almost 62.5% from the case when no backaction is taken into account. Hence, we simulate the magnetic trapping of the flux qubit above the spherical magnet in the commercial finite element method (FEM) package COMSOL. We find FEM simulation results for the Meissner trapping of an SC sphere which match very well with the analytical solutions (see [SM] for more details).

Using FEM simulation, we find that the large ring-like flux qubit experience complete rigid-body trapping (see [SM] for more details), and we present the results in Fig. 4. We find comparable results based on analytical solutions from reference [54] (see [SM] for more details). In Fig. 4 (a), we present one of the examples from our FEM simulations showing the cross-section of magnetic trapping of the flux qubit. From 4(a), we can see that the magnetic field strength at the location of the ring is very small ( $|B| < 1$  mT) and this ensures proper working of the flux qubit in our scheme. Furthermore, we observe significant perturbation of the fields surrounding the flux-qubit which is expected due to the backaction of the superconducting ring. From the cross-section plot Fig. 4(a), we can see that as  $R$  (the flux-qubit radius) increases, the magnetic field seen by the flux qubit decreases and we expect the trapping stiffness (and thereby the  $\omega_z$  and  $h$ ) to drop as  $R$  increases. We identify this region of  $R$  as shown in Fig. 4(b) and (c), there is a critical value of the radius above which the flux qubit cannot be stably trapped. We show the resultant

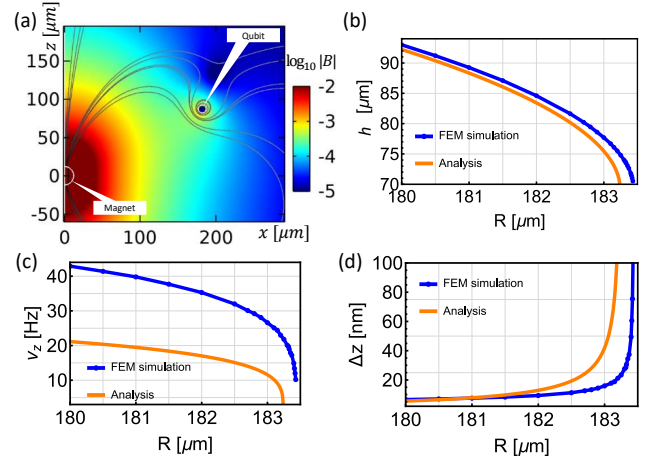


FIG. 4. Numerical FEM simulation results of the trapped superconducting flux qubit and its motional superposition. (a) Magnetic flux density  $B$  in the radial plane for a magnetic trap where a flux qubit of radius  $R = 183.4 \mu\text{m}$  is levitated  $h = 71.8 \mu\text{m}$  above a spherical magnet with a radius of  $r = 12 \mu\text{m}$ . We can see the back-action of the Meissner expulsion on the  $B$  field around the levitated flux qubit. With the increase of the radius, the vertical equilibrium position and trap frequency will decrease, and the spatial superposition separation will increase therewith. There is a critical point for the radius, above which the trap is unstable. When the radius is chosen to be  $R = 183.4 \mu\text{m}$ , we can get a stable trap with vertical trap frequency  $\nu_z = 15 \text{ Hz}$ , achieving spatial superposition separation of  $\Delta z = 100 \text{ nm}$  and  $\chi \sim 10^6$ . For qualitative comparison, analytical solutions are plotted in orange curves. Please see the main text for more details.

massive spatial superposition in this region, in Fig. 4(d). We obtain a massive spatial superposition of  $\Delta z \sim 100 \text{ nm}$ , when  $\nu_z \sim 15 \text{ Hz}$  for a radius of  $183.4 \mu\text{m}$  and the corresponding  $\chi \sim 10^6$  with a Q-factor of around  $Q \sim 2.8 \times 10^7$ . Larger values of  $\Delta z$  are predicted from theory but are probably not feasible in experiments due to potential instabilities in a very low-frequency trap.

**Conclusion** – In this letter, we have introduced two magnetically-driven methods to achieve macroscopic motional superposition states for massive objects. In the first method, a levitated YIG microsphere with a motional  $Q \sim 10^8$ , can be driven into motional superposition state using adjacent magnetic flux qubits at both sides of the trapped YIG to apply quantum magnetic forces. The results show that the superposition spatial separation is independent of the size of the YIG particle in principle. In the second part, we propose a reversed scheme where the macroscopic spatial superposition can be realized directly on a flux qubit that is levitated above a magnetic microsphere, with a ring motional  $Q \sim 10^7$ . In both the schemes, massive superposition separation extents reach the extreme value  $\chi \sim 10^6$ . One needs to maximize the motional Q-factor to permit coherent dynamics for a duration long enough to prepare the superposition state and thereby utilise such large superposition states for quantum sensing applications [38]. The motional Q-factor can be improved further by working at even further low pressure ( $P_g < 10^{-11} \text{ mbar}$ ), by keeping the low frequency considered in this work. With improved flux qubit coherence times,



both these macroscopic motional superposition states could be achieved experimentally which can pave the way to explore more fundamental quantum physics and ultra-sensitive applications.

*Acknowledgement*— This work was supported by Australian Research Council centre of Excellence for Engineered Quantum Systems (CE170100009) and the Okinawa Institute for Science and Technology Graduate University.

- 
- [1] E. Schrödinger, Die gegenwärtige Situation in der Quantenmechanik, *Die Naturwissenschaften* **23**, 807 (1935).
  - [2] R. Penrose, On gravity's role in quantum state reduction, *General Relativity and Gravitation* **28**, 581 (1996).
  - [3] A. Bassi, K. Lochan, S. Satin, T. P. Singh, and H. Ulbricht, Models of wave-function collapse, underlying theories, and experimental tests, *Reviews of Modern Physics* **85**, 471 (2013).
  - [4] A. Vinante, R. Mezzena, P. Falferi, M. Carlesso, and A. Bassi, Improved Noninterferometric Test of Collapse Models Using Ultracold Cantilevers, *Physical Review Letters* **119**, 110401 (2017).
  - [5] B. Helou, B. J. J. Slagmolen, D. E. McClelland, and Y. Chen, LISA Pathfinder appreciably constrains collapse models, *Physical Review D* **95**, 084054 (2017).
  - [6] D. Zheng, Y. Leng, X. Kong, R. Li, Z. Wang, X. Luo, J. Zhao, C.-K. Duan, P. Huang, J. Du, M. Carlesso, and A. Bassi, Room temperature test of the continuous spontaneous localization model using a levitated micro-oscillator, *Physical Review Research* **2**, 58 (2020).
  - [7] S. Bose, Matter wave ramsey interferometry and the quantum nature of gravity, Available at [https://www.youtube.com/watch?v=0Fv-0k13s\\_k](https://www.youtube.com/watch?v=0Fv-0k13s_k) (2016), fundamental Problems of Quantum Physics, ICTS, Bangalore.
  - [8] S. Bose, A. Mazumdar, G. W. Morley, H. Ulbricht, M. Toroš, M. Paternostro, A. A. Geraci, P. F. Barker, M. S. Kim, and G. Milburn, Spin Entanglement Witness for Quantum Gravity, *Physical Review Letters* **119**, 240401 (2017).
  - [9] C. Marletto and V. Vedral, Gravitationally Induced Entanglement between Two Massive Particles is Sufficient Evidence of Quantum Effects in Gravity, *Physical Review Letters* **119**, 240042 (2017).
  - [10] G. Bhole, J. A. Jones, C. Marletto, and V. Vedral, Witnesses of non-classicality for simulated hybrid quantum systems, *Journal of Physics Communications* **4**, 025013 (2020).
  - [11] R. J. Marshman, A. Mazumdar, and S. Bose, Locality and entanglement in table-top testing of the quantum nature of linearized gravity, *Physical Review A* **101**, 052110 (2020).
  - [12] M. Toroš, T. W. van de Kamp, R. J. Marshman, M. Kim, A. Mazumdar, and S. Bose, Relative acceleration noise mitigation for entangling masses via quantum gravity, *arXiv preprint arXiv:2007.15029* (2020).
  - [13] S. Bose, A. Mazumdar, M. Schut, and M. Toroš, Mechanism for the quantum natured gravitons to entangle masses, *Physical Review D* **105**, 106028 (2022).
  - [14] N. Altamirano, P. Corona-Ugalde, R. B. Mann, and M. Zych, Gravity is not a pairwise local classical channel, *Classical and Quantum Gravity* **35**, 145005 (2018).
  - [15] M. J. W. Hall and M. Reginatto, On two recent proposals for witnessing nonclassical gravity, *Journal of Physics A: Mathematical and Theoretical* **51**, 085303 (2018).
  - [16] A. Belenchia, R. M. Wald, F. Giacomini, E. Castro-Ruiz, A. Brukner, and M. Aspelmeyer, Information content of the gravitational field of a quantum superposition, *International Journal of Modern Physics D* **28**, 1 (2019).
  - [17] M. Carlesso, A. Bassi, M. Paternostro, and H. Ulbricht, Testing the gravitational field generated by a quantum superposition, *New Journal of Physics* **21**, 093052 (2019).
  - [18] M. Christodoulou and C. Rovelli, On the possibility of laboratory evidence for quantum superposition of geometries, *Physics Letters, Section B: Nuclear, Elementary Particle and High-Energy Physics* **792**, 64 (2019).
  - [19] H. C. Nguyen and F. Bernards, Entanglement dynamics of two mesoscopic objects with gravitational interaction, *European Physical Journal D* **74**, 2 (2020).
  - [20] T. Krisnanda, G. Y. Tham, M. Paternostro, and T. Paterek, Observable quantum entanglement due to gravity, *npj Quantum Information* **6**, 4 (2020).
  - [21] M. Arndt and K. Hornberger, Testing the limits of quantum mechanical superpositions, *Nature Physics* **10**, 271 (2014).
  - [22] Y. Y. Fein, P. Geyer, P. Zwick, F. Kiałka, S. Pedalino, M. Mayor, S. Gerlich, and M. Arndt, Quantum superposition of molecules beyond 25 kDa, *Nature Physics* **15**, 1242 (2019).
  - [23] M. Scala, M. Kim, G. Morley, P. Barker, and S. Bose, Matter-wave interferometry of a levitated thermal nano-oscillator induced and probed by a spin, *Physical review letters* **111**, 180403 (2013).
  - [24] C. Wan, M. Scala, G. Morley, A. A. Rahman, H. Ulbricht, J. Bateman, P. Barker, S. Bose, and M. Kim, Free nano-object ramsey interferometry for large quantum superpositions, *Physical review letters* **117**, 143003 (2016).
  - [25] Y. Margalit, O. Dobkowski, Z. Zhou, O. Amit, Y. Japha, S. Moukouri, D. Rohrlach, A. Mazumdar, S. Bose, C. Henkel, *et al.*, Realization of a complete stern-gerlach interferometer: Toward a test of quantum gravity, *Science advances* **7**, eabg2879 (2021).
  - [26] B. Wood, S. Bose, and G. Morley, Spin dynamical decoupling for generating macroscopic superpositions of a free-falling nanodiamond, *Physical Review A* **105**, 012824 (2022).
  - [27] R. J. Marshman, A. Mazumdar, R. Folman, and S. Bose, Constructing nano-object quantum superpositions with a stern-gerlach interferometer, *Physical Review Research* **4**, 023087 (2022).
  - [28] R. Zhou, R. J. Marshman, S. Bose, and A. Mazumdar, Mass independent scheme for large spatial quantum superpositions, *arXiv preprint arXiv:2210.05689* (2022).
  - [29] S. Bose, K. Jacobs, and P. L. Knight, Preparation of nonclassical states in cavities with a moving mirror, *Physical Review A - Atomic, Molecular, and Optical Physics* **56**, 4175 (1997).
  - [30] Z.-q. Yin, T. Li, X. Zhang, and L. M. Duan, Large quantum superpositions of a levitated nanodiamond through spin-optomechanical coupling, *Physical Review A* **88**, 033614 (2013).
  - [31] D. Lombardo and J. Twamley, Deterministic Creation of Macroscopic Cat States, *Scientific Reports* **5**, 13884 (2015).
  - [32] J.-Q. Liao and L. Tian, Macroscopic Quantum Superposition in Cavity Optomechanics, *Physical Review Letters* **116**, 163602 (2016).
  - [33] J. Clarke and M. R. Vanner, Growing macroscopic superposition states via cavity quantum optomechanics, *Quantum Sci-*

- ence and Technology **4**, 014003 (2018).
- [34] H. Xie, X. Shang, C. G. Liao, Z. H. Chen, and X. M. Lin, Macroscopic superposition states of a mechanical oscillator in an optomechanical system with quadratic coupling, *Physical Review A* **100**, 33803 (2019).
  - [35] L. Zheng, D. N. Chen, Z. Y. Peng, Y. Shi, Y. J. Liu, and Y. D. Wang, Macroscopic Quantum Superposition in Optomechanical System with Ultrastrong Coupling Light-Matter Interaction, *International Journal of Theoretical Physics* **59**, 824 (2020).
  - [36] I. Shomroni, L. Qiu, and T. J. Kippenberg, Optomechanical generation of a mechanical catlike state by phonon subtraction, *Physical Review A* **101**, 033812 (2020).
  - [37] H. Zhan, G. Li, and H. Tan, Preparing macroscopic mechanical quantum superpositions via photon detection, *Physical Review A* **101**, 063834 (2020).
  - [38] M. T. Johnsson, G. K. Brennen, and J. Twamley, Macroscopic superpositions and gravimetry with quantum magnetomechanics, *Scientific Reports* **6**, 37495 (2016).
  - [39] O. Romero-Isart, Coherent inflation for large quantum superpositions of levitated microspheres, *New Journal of Physics* **19**, 123029 (2017).
  - [40] A. T. M. A. Rahman, Large spatial Schrödinger cat state using a levitated ferrimagnetic nanoparticle, *New Journal of Physics* **21**, 113011 (2019).
  - [41] W. Qin, A. Miranowicz, G. Long, J. Q. You, and F. Nori, Proposal to test quantum wave-particle superposition on massive mechanical resonators, *npj Quantum Information* **5**, 58 (2019).
  - [42] J. S. Pedernales, G. W. Morley, and M. B. Plenio, Motional Dynamical Decoupling for Interferometry with Macroscopic Particles, *Physical Review Letters* **125**, 23602 (2020).
  - [43] T. Kovachy, P. Asenbaum, C. Overstreet, C. A. Donnelly, S. M. Dickerson, A. Sugarbaker, J. M. Hogan, and M. A. Kasevich, Quantum superposition at the half-metre scale, *Nature* **528**, 530 (2015).
  - [44] L. Pezzè, M. Gessner, P. Feldmann, C. Klempt, L. Santos, and A. Smerzi, Heralded Generation of Macroscopic Superposition States in a Spinor Bose-Einstein Condensate, *Physical Review Letters* **123**, 260403 (2019).
  - [45] M. Bild, M. Fadel, Y. Yang, U. von Lüpke, P. Martin, A. Bruno, and Y. Chu, Schrödinger cat states of a 16-microgram mechanical oscillator, *Science* **380**, 274 (2023).
  - [46] M. Cirio, G. K. Brennen, and J. Twamley, Quantum magnetomechanics: Ultrahigh-Q-levitated mechanical oscillators, *Physical Review Letters* **109**, 147206 (2012).
  - [47] S. Caplan and G. Chanin, Critical-Field Study of Superconducting Aluminum, *Physical Review* **138**, A1428 (1965).
  - [48] M. T. Johnsson, G. K. Brennen, and J. Twamley, Macroscopic superpositions and gravimetry with quantum magnetomechanics, *Scientific Reports* **6**, 37495 (2016).
  - [49] C. Gonzalez-Ballester, M. Aspelmeyer, L. Novotny, R. Quidant, and O. Romero-Isart, Levitodynamics: Levitation and control of microscopic objects in vacuum, *Science* **374**, 168 (2021).
  - [50] D. E. Chang, C. A. Regal, S. B. Papp, D. J. Wilson, J. Ye, O. Painter, H. J. Kimble, and P. Zoller, Cavity opto-mechanics using an optically levitated nanosphere, *Proceedings of the National Academy of Sciences* **107**, 1005 (2010).
  - [51] T. Wang, S. Lourette, S. R. O'Kelley, M. Kayci, Y. Band, D. F. J. Kimball, A. O. Sushkov, and D. Budker, Dynamics of a Ferromagnetic Particle Levitated over a Superconductor, *Physical Review Applied* **11**, 044041 (2019).
  - [52] B. De Lima Bernardo, F. Moraes, and A. Rosas, Drag force experienced by a body moving through a rarefied gas, *Chinese Journal of Physics* **51**, 189 (2013).
  - [53] J. Gieseler, A. Kabcenell, E. Rosenfeld, J. D. Schaefer, A. Safira, M. J. Schuetz, C. Gonzalez-Ballester, C. C. Rusconi, O. Romero-Isart, and M. D. Lukin, Single-Spin Magnetomechanics with Levitated Micromagnets, *Physical Review Letters* **124**, 163604 (2020).
  - [54] C. Navau, S. Minniberger, M. Trupke, and A. Sanchez, Levitation of superconducting microrings for quantum magnetomechanics, *Physical Review B* **103**, 174436 (2021).

# Supplementary information for massive quantum superpositions using magneto-mechanics

Sarath Raman Nair,<sup>1,2,\*</sup> Shilu Tian,<sup>3,†</sup> Gavin K. Brennen,<sup>1,2</sup> Sougato Bose,<sup>4</sup> and Jason Twamley<sup>3,‡</sup>

<sup>1</sup>*School of Mathematical and Physical Sciences, Macquarie University, NSW 2109, Australia*

<sup>2</sup>*ARC Centre of Excellence for Engineered Quantum Systems (EQUS), Macquarie University, NSW 2109, Australia*

<sup>3</sup>*Quantum Machines Unit, Okinawa Institute of Science and Technology Graduate University, Onna, Okinawa 904-0495, Japan*

<sup>4</sup>*Department of Physics and Astronomy, University College London, Gower Street, WC1E 6BT London, UK*

## I. Q-FACTOR ESTIMATION

We assume that the main source of damping of the oscillator in our schemes is the collision of gas molecules surrounding the oscillator onto the oscillator. Then the Quality factor which determines how long the oscillator can coherently oscillate in its ground state can be written generally as [1],

$$Q = \frac{\pi}{4} \rho \omega_z^2 A \frac{V}{\bar{F}_g} \quad (1)$$

where  $\rho$ ,  $V$  is the volume of the oscillator respectively,  $\omega_z$  and  $A$  are the frequency and amplitude of the oscillation respectively. The term  $\bar{F}_g$  is the drag force due to the collision of the oscillator with surrounding molecules. This parameter depends on the geometry of the oscillator [2]. In order to estimate this parameter  $\bar{F}_g$ , we first assume that the velocity of the oscillator moving in the gas is much smaller than the surrounding gas molecules as in [1]. Then an equation, if the oscillator is a spherical body the Q-factor is already worked out in [1]. In the case of flux qubit as the oscillator, we make the following assumption. The flux qubit is a toroid in a cross-sectional radius  $r$  and a length of  $2\pi R$ , where  $R$  is the radius of the flux qubit. We can assume this toroid as  $N$  cylinders, each with a length of  $2\pi R/N$ . Then we can assume that these  $N$  cylinders are moving in the gas along the direction perpendicular to the normal of the cross-sectional area. The collision of the gas molecules happens at the curved surfaces of the cylinders. The relative angle between the cylinders is not expected to make any difference. The total force is the force on each cylinder multiplied by the  $N$ . Which is equal to treating the toroid as a single cylinder with a length of  $2\pi R$ . From references [1, 2], the  $V/\bar{F}_g$  can be written for both these two cases as,

$$\frac{V}{\bar{F}_g} = \frac{2r}{3} \sqrt{\frac{3k_B T}{M_g}} \frac{1}{P_g \omega_z A} \quad (2)$$

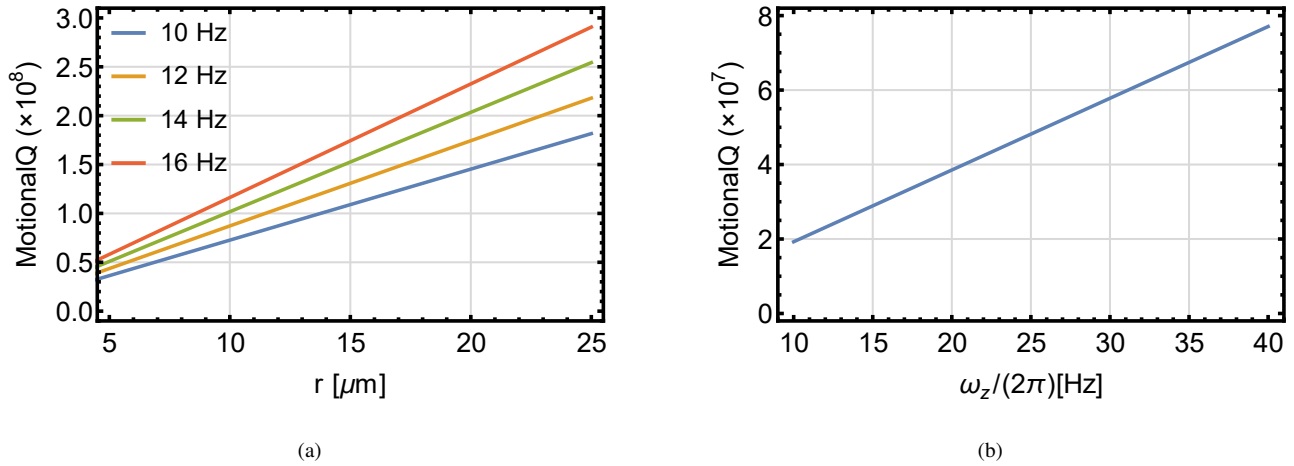


FIG. 1. Q-factor of the oscillator for the damping due to the gas collision (a) Q-factor as a function of YIG sphere radius for different  $\omega/(2\pi)$  values as denoted in the plot legends. (b) Q-factor as a function of the trap frequency for the flux qubit considered in the magnetic levitation of flux qubit scheme. Please see the table below in this supplementary material for the numerical values of the parameters used.

\* Joint first authors; Corresponding author : sarath.raman-nair@mq.edu.au

† Joint first authors

‡ Corresponding author : jason.twamley@oist.jp

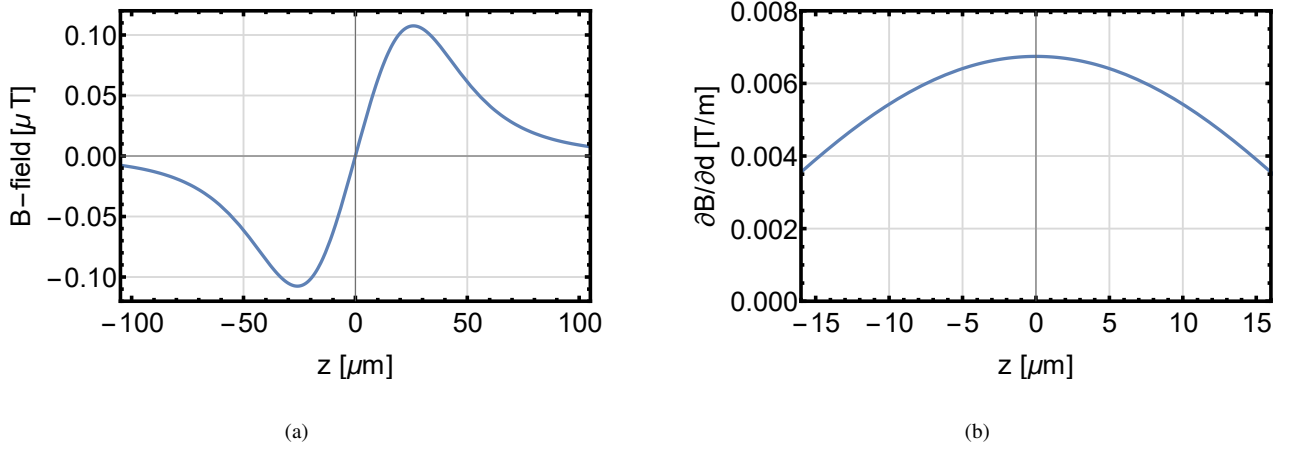


FIG. 2. Magnetic field (in (a)) and its gradient (in (b)) generated by the flux qubits as a function of distance from the origin ( $z$ ) for  $R = 40\mu\text{m}$ , based on Eq. (4) and Eq. (5).

where  $P_g$  is the pressure of the gas,  $k_B$  is the Boltzmann's constant,  $T$  is the temperature at which the experiments are performed,  $M_g$  is the mass of the gas molecule. Here  $r$  is the radius for the spherical resonator and for the toroid resonator, it is the cross-sectional radius. Using Eq. (3) and Eq. (2), we obtain the Q-factor as,

$$Q = \frac{\pi}{6} \frac{\rho r \omega_z}{P_g} \sqrt{\frac{3k_B T}{M_g}} \quad (3)$$

Assuming Helium as the gas is present in the surroundings we estimate the Q-factor for the optically levitated YIG sphere and the magnetically levitated flux qubit and the results are presented in Fig. 1.

## II. ANALYTICAL MODELING OF MOTIONAL SUPERPOSITION OF A TRAPPED CRYSTALLINE MAGNETIC MICROSPHERE

We describe the details of analytical modeling of the generation of a macroscopic quantum superposition using the flux-qubit magnetic actuation of a trapped YIG nanoparticle.

### A. Modelling the flux qubit as Solenoid

We model the two flux qubits as superconducting rings as mentioned in the main text. For this we assume that these rings have radii of  $R$  each and each of these flux qubits is symmetrically located at a distance  $z_{\pm}^{FQ} = \pm\eta R$ , along the  $z$ -axis around the origin, where  $\eta$  is a dimensionless scaling factor. The flux qubits have supercurrents  $I$  circulating in each ring. We can write down the magnetic field generated by the two superconducting flux qubits at a point on the  $z$ -axis  $\vec{r} = (0, 0, z)$  as,

$$\vec{B}(z) = \frac{\mu_0 I R^2}{2} \left( \frac{1}{((z - \eta R)^2 + R^2)^{3/2}} - \frac{1}{((z + \eta R)^2 + R^2)^{3/2}} \right) \hat{z}, \quad (4)$$

where  $\mu_0$  is the vacuum permeability. The gradient of the magnetic field can be obtained as,

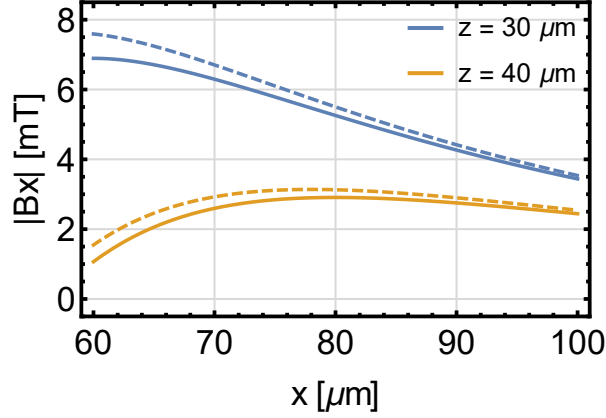
$$\frac{\partial \vec{B}}{\partial z} = -\frac{3\mu_0 I R^2}{2} \left( \frac{(z - \eta R)}{((z - \eta R)^2 + R^2)^{5/2}} - \frac{(z + \eta R)}{((z + \eta R)^2 + R^2)^{5/2}} \right) \hat{z}, \quad (5)$$

The numerical solutions for the magnetic field and its gradient from two superconducting flux qubits using equations (4) and (5) are shown in Figure 2. From the numerical solutions in 2, we can see that the magnetic field varies linearly and the gradient of the magnetic field is constant for small displacements.

At the origin ( $z = 0$ ) the magnetic field gradient is,

$$\frac{\partial \vec{B}}{\partial z} = \frac{3\mu_0 I}{R^2} \frac{\eta}{(1 + \eta^2)^{5/2}} \hat{z}, \quad (6)$$





(a)

FIG. 3. Absolute value of B-field as a function of x position for two different z positions as denoted by the plot legends. The solid curves correspond to the magnetic sphere at the origin and the dashed curves correspond to when the magnetic sphere is shifted to  $z = 1 \mu m$ .

We find by maximizing  $\eta/(1 + \eta^2)^{5/2}$  that this non-vanishing magnetic field gradient is maximum when the flux qubits are on each side of the YIG sphere with  $\eta = 0.5$ .

From Fig. 2, we can see that the magnetic field strength is linearly varying around  $z = 0$  such that we can approximate  $B \sim \frac{\partial B}{\partial z} z$  for small displacements.

### B. Analytical solution for the equilibrium position

We consider a spherical magnet (for example a YIG sphere) trapped in three dimensions. The experimental demonstration of it via magnetic levitation can be found in the references [1][3][4][5]. Assuming the trap to be a harmonic trap along all the axis, we can express the optical force on the z-axis defined in the main text as,  $\vec{F}_{TR} = -\hat{z}\rho V\omega_z^2 z$  [6]. The magnetic force on the YIG sphere due to the flux qubit state using dipole model is,  $\vec{F}_{FQ}^{(q)} = \vec{m}_0 \cdot (\partial \vec{B}_z / \partial z)|_q$ . We approximate the YIG nanosphere as a point dipole due to its spherical shape and thus can write its dipole moment as,  $\vec{m}_0 = \mu_0^{-1} B_r V \hat{z}$ . Here the  $B_r$  is the remnant magnetic field of the YIG sphere. Due to the trapping and magnetic actuation force on the YIG sphere, it moves to a new equilibrium position in the optical trap where it satisfies,  $\vec{F}_{FQ}^{(q)} + \vec{F}_{TR} = 0$ . We can write down this condition as,

$$\frac{B_r}{\mu_0} V \left( \frac{\partial \vec{B}_z}{\partial z} \right)_{|q\rangle} - \rho V \omega_z^2 z_{eq} = 0 \quad (7)$$

Using equation (5), for  $|0\rangle$ , we can write equation (7) as,

$$\frac{3IB_r R^2}{\rho \omega_z^2} \left( \frac{(z_{eq} - (R/2))}{((z_{eq} - (R/2))^2 + R^2)^{5/2}} - \frac{(z_{eq} + (R/2))}{((z_{eq} + (R/2))^2 + R^2)^{5/2}} \right) + z_{eq} = 0, \quad (8)$$

where we considered  $\eta = 1/2$ . Then for the superposition of  $|0\rangle$  and  $|1\rangle$ , we can obtain spatial superposition extent as,  $\Delta z = 2z_{eq}$ . We can write Eq. (8) using the transformation  $z_{eq} \rightarrow (\Delta z/2)$  to obtain an equation in terms of  $\Delta z$  for numerical calculations as,

$$\frac{3IB_r R^2}{\rho \omega_z^2} \left( \frac{((\Delta z/2) - (R/2))}{(((\Delta z/2) - (R/2))^2 + R^2)^{5/2}} - \frac{((\Delta z/2) + (R/2))}{(((\Delta z/2) + (R/2))^2 + R^2)^{5/2}} \right) + (\Delta z/2) = 0. \quad (9)$$

### C. Magnetic field generated by spherical magnet

We assumed that the magnetic field produced by the spherical magnet at the location of the superconducting material is below the critical magnetic field of 9.8 mT for Aluminium. To verify this assumption, we have modeled a spherical magnet of radius  $25 \mu m$  (Other parameters are in the Table I below), using Radia in Mathematica [7]. We applied linear anisotropic material for the spherical magnet in the Radia model, with the parallel and perpendicular magnetic field susceptibility of 1 and 0 respectively,

with the remnant magnetic field of YIG along the z-axis. We simulated the B-field along the x-axis at  $z = 30 \mu m$  and  $z = 40 \mu m$  for a sphere magnet at the origin and also for a sphere located at  $z = 1 \mu m$  (Please see FIG. 1 in the main text). The results are shown in Fig. 3 and from these results, we can see that the assumption is correct for any shifts within the range presented here.

### III. TRAPPING SUPERCONDUCTING FLUX QUBIT USING SPHERICAL MAGNET

In this section, we discuss the details of the scheme to generate spatial superposition using magnetically levitated flux qubit.

#### A. Analytical solution for trapping superconducting flux qubit above the spherical magnet

We approximate the levitation of flux qubit above the spherical magnet to the levitation of a superconducting ring using a point dipole as the spherical magnet can be approximated as a point dipole. An analytical framework for estimating the trap frequency and equilibrium position for this problem of levitating a superconducting ring by a point dipole has been developed in reference [8]. We first assume a coordinate system where the magnet is at the origin of the coordinate system and the magnetic trapping axis of the flux qubit is along  $+\hat{z}$ . Based on the analytical results by reference [8], the equilibrium position,  $h$  for the flux qubit ring in the Meissner state levitated by the spherical micromagnet can then be obtained by solving the equation,

$$\frac{16\pi^2 r^2 g \rho}{\mu_0^2 m_{mag}^2} R^5 (\ln [8R/r] - 2) - \frac{6(h/R)}{(1 + (h/R)^2)^4} = 0, \quad (10)$$

where  $R$ ,  $\rho$ , and  $r$  are the radius, density, and cross-sectional radius of the flux qubit, respectively; and  $m_{mag}$  is the magnetic moment of the magnet and  $g$  is the gravity acceleration constant. For a stable levitation, the dimensionless term  $(16\pi^2 r^2 g \rho / \mu_0^2 m_{mag}^2) R^5 (\ln [8R/r] - 2)$  in 10, should be less than 1.329 [8]. This sets an upper bound for the flux qubit radius  $R$  for a fixed cross-sectional radius  $r$ . Using the equilibrium position obtained from 10, we can estimate the trap frequency in Hz, along the trapping axis  $\nu_z$  using the equation [8],

$$\nu_z = \sqrt{\frac{3\mu_0 m_{mag}^2 (7(h/R)^2 - 1)}{128\pi^4 r^2 \rho R^4 (\ln [8R/r] - 2) (1 + (h/R)^2)^5}}. \quad (11)$$

For the easiness of analysis, we shift the origin of the coordinate system from the spherical magnet to the equilibrium position,  $h$  of the levitated flux qubit with the transformation  $(x, y, z) \rightarrow (x, y, z + h)$ .

Driving the qubit inductively a supercurrent flow can be induced that we denote as  $I$ . Then depending on the direction of flow qubit can be put into  $|0\rangle$  or  $|1\rangle$  state in the levitated flux qubits. Then the flux qubit acquires a resultant dipole moment,  $\vec{m}_{sc} = \hat{z} I \pi R^2$  ( $\vec{m}_{sc} = -\hat{z} I \pi R^2$ ), which points downward (upward) the qubit is in the  $|0\rangle$  ( $|1\rangle$ ) state with  $I$  flows clockwise (counterclockwise) direction. The levitated flux qubit with the magnetic moment  $\vec{m}_{sc}$ , then experiences a force for being in one of the qubit states,  $\vec{F}_{FQ} = \vec{m}_{sc} \cdot (\partial \vec{B}_z / \partial z)$ . When the qubit is in  $|0\rangle$  ( $|1\rangle$ ) state, the flux qubit experiences a  $\vec{F}_{FQ} = \hat{z} 3\mu_0 m_{mag} I R^2 / (2(z + h)^4)$  ( $\vec{F}_{FQ} = -\hat{z} 3\mu_0 m_{mag} I R^2 / (2(z + h)^4)$ ). Due to this  $\vec{F}_{FQ}$  and the equilibrium position shifts to a position,  $z_{eq}$  where the  $\vec{F}_{FQ}$  is balanced by the magnetic trapping force  $\vec{F}_{TR} = -\hat{z} 8\pi^4 r^2 \rho R \nu_z^2 z_{eq}$ . At equilibrium position,  $\vec{F}_{FQ} + \vec{F}_{TR} = 0$ . Please note that the effect of gravitational force is already included in the magnetic trapping force. For  $z_{eq} \ll h$ , the equilibrium position is obtained analytically as,

$$z_{eq} \sim \frac{3\mu_0 m_{mag} I R^2}{16\pi^2 r^2 \rho \nu_z^2 h^4}. \quad (12)$$

Then the  $\Delta z = 2z_{eq}$ .

#### B. Trapping a superconducting sphere between two dipoles

We show the back-action effect of the superconductor on the magnetic field used to trap it by considering the example of trapping a superconducting (SC) sphere using two dipoles in an anti-Helmholtz magnetic configuration (magnetic moments anti-parallel). This anti-Helmholtz magnetic configuration can be realised experimentally either using current carrying loops as in the section for introducing the first method or using uniformly magnetised spherical magnets to produce an external magnetic field that is identical to a point magnetic dipole [9].

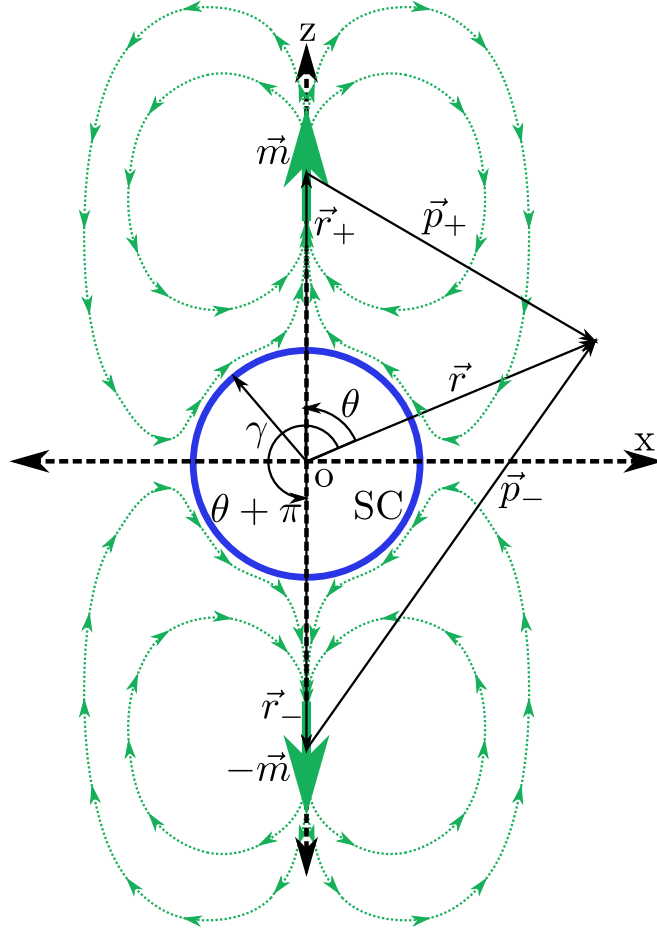


FIG. 4. Schematic diagram for the analytical derivation of the magnetic trap properties in  $z$  direction. The SC sphere with radius  $\gamma$  located at the origin  $o$  is shown in blue circle. Magnetic dipoles with moment  $\vec{m}$  and  $-\vec{m}$  are shown in thick green arrows and their field lines are represented in green dotted arrows.  $\vec{r}_+$  and  $\vec{r}_-$  are the vectors from origin to magnetic dipoles  $\vec{m}$  and  $-\vec{m}$  respectively. An arbitrary point is chosen for generalized derivation and the  $\vec{r}$  is shown from the origin to this arbitrary point.  $\vec{p}_+$  and  $\vec{p}_-$  are respectively the vectors from magnetic dipoles  $\vec{m}$  and  $-\vec{m}$  to the arbitrary point of interest.

We first note that a number of authors have considered analytic treatments of the Meissner force of a SC sphere in anti-Helmholtz magnetic fields [10, 11], as well as the force between a point dipole and a SC sphere [12, 13]. Many of these works use the image method but there seems to be some concern in the literature regarding this method [14], and so we do not use the image method in what follows and solve for the magnetic fields and associated forces directly.

We consider the magnets and SC sphere to have centers that all lie on the  $z$ -axis, and visualise the geometry in the  $x-z$  plane as shown in Figure 4. We analytically derive the induced magnetic field at the SC sphere due to the magnetic field of the two point dipoles, using scalar potentials of the dipoles and enforcing the appropriate boundary conditions at the surface of the SC sphere. Then we derive an expression for the levitation force by considering the interaction between the resulting magnetic field and the two point dipoles.

We denote  $\Phi_+$ , and  $\Phi_-$ , to be the scalar potentials of the two dipoles located respectively at  $\vec{r}_+ \sim (0, 0, d_+)$  and  $\vec{r}_- \sim (0, 0, -d_-)$ , at either side of the origin along the  $z$ -axis. At the arbitrary point  $\vec{r} \sim (x, y, z)$ , these scalar potentials can be written as [12, 15],

$$\Phi_{\pm}(\vec{r}) = \pm \frac{\mu_0}{4\pi} \frac{\vec{m} \cdot \vec{p}_{\pm}}{||\vec{p}_{\pm}||^3}, \quad (13)$$

where  $\mu_0$  is the magnetic permeability of free space and  $\vec{p}_{\pm} = \vec{r} - \vec{r}_{\pm}$ . In spherical coordinates with  $\vec{r}$  radius,  $\theta$  as polar angle and  $\phi$  azimuthal angle, equations (13) can be rewritten as,

$$\Phi_{\pm}(\tilde{r}_{\pm}, \theta) = \frac{\mu_0 m}{4\pi d_{\pm}^2} \frac{((\pm \tilde{r}_{\pm}) \cos \theta - 1)}{\left((\pm \tilde{r}_{\pm})^2 - 2(\pm \tilde{r}_{\pm}) \cos \theta + 1\right)^{\frac{3}{2}}}, \quad (14)$$

Here,  $m = ||\vec{m}||$ ,  $\tilde{r}_\pm = r/d_\pm$ . There is no  $\phi$  dependency due to the axial symmetry of the system. Expanding using Legendre polynomials, (14) can be written as,

$$\Phi_\pm(\tilde{r}_\pm, \theta) = -\frac{\mu_0 m}{4\pi d_\pm^2} \sum_{n=0}^{\infty} (n+1) (\pm \tilde{r}_\pm)^n P_n(\cos \theta), \quad (15)$$

Then the net scalar potential ( $\Phi_m \equiv \Phi_+ + \Phi_-$ ), generated by the two dipoles can be written as,

$$\Phi_m(r, \theta) = -\frac{\mu_0 m}{4\pi} \sum_{n=0}^{\infty} (n+1) r^n P_n(\cos \theta) \left[ \left( \frac{1}{d_+} \right)^{n+2} + \left( -\frac{1}{d_-} \right)^{n+2} \right]. \quad (16)$$

The radial component of the magnetic field generated by the two dipoles is given by,  $\vec{B}_{r,m} = -\hat{r} \frac{\partial \Phi_m}{\partial r}$  and in our case we find,

$$\vec{B}_{r,m}(r, \theta) = \hat{r} \frac{\mu_0 m}{4\pi} \sum_{n=0}^{\infty} n(n+1) r^{(n-1)} P_n(\cos \theta) \left[ \left( \frac{1}{d_+} \right)^{n+2} + \left( -\frac{1}{d_-} \right)^{n+2} \right], \quad (17)$$

We use the subscript r to indicate that we only compute the radial component of  $\vec{B}$  and the m subscript indicates that the magnetic field is due to the dipoles and without the SC sphere. Introducing the SC sphere results in the introduction of an additional effective magnetic field in response to the field due to the dipoles. Taken together, the induced and dipole fields must satisfy the Meissner boundary conditions, that the total magnetic field has a vanishing orthogonal component at all superconducting surfaces.

We write down a general solution for the scalar potential corresponding to an induced magnetic field of the SC sphere, due to the Meissner effect as,

$$\Phi_{SC}(r, \theta) = \sum_{n=0}^{\infty} \frac{C_n}{r^{(n+1)}} P_n(\cos \theta); \quad r > \gamma, \quad (18)$$

where  $C_n$  is a general coefficient that has to be determined and  $\gamma$  is the radius of the SC sphere. This gives a magnetic field in the radial direction as,

$$\vec{B}_{r,SC}(r, \theta) = \hat{r} \sum_{n=0}^{\infty} (n+1) \frac{C_n}{r^{(n+2)}} P_n(\cos \theta). \quad (19)$$

We now express the total radial component of the magnetic field as,  $\vec{B}_{r,T} = \vec{B}_{r,m} + \vec{B}_{r,SC}$ . Considering the perfect Meissner state for the SC sphere, we must have  $\vec{B}_{r,T}(r = \gamma, \theta) = 0 \forall \theta$ . This permits us to fix  $C_n$  to be,

$$C_n = -\frac{\mu_0 m}{4\pi} n \gamma^{(2n+1)} \left[ \left( \frac{1}{d_+} \right)^{n+2} + \left( -\frac{1}{d_-} \right)^{n+2} \right]. \quad (20)$$

Inserting equation (20) into equation (18) and equation (19), we obtain the scalar potential and the radial component of the induced magnetic field of SC sphere as,

$$\Phi_{SC}(r, \theta) = -\frac{\mu_0 m}{4\pi} \sum_{n=0}^{\infty} n \frac{\gamma^{(2n+1)}}{r^{(n+1)}} P_n(\cos \theta) \left[ \left( \frac{1}{d_+} \right)^{n+2} + \left( -\frac{1}{d_-} \right)^{n+2} \right], \quad (21)$$

$$\vec{B}_{r,SC}(r, \theta) = -\hat{r} \frac{\mu_0 m}{4\pi} \sum_{n=0}^{\infty} n(n+1) \frac{\gamma^{(2n+1)}}{r^{(n+2)}} P_n(\cos \theta) \left[ \left( \frac{1}{d_+} \right)^{n+2} + \left( -\frac{1}{d_-} \right)^{n+2} \right]. \quad (22)$$

Choosing  $\theta = 0$  and  $\pi$ , the magnetic field at the location of the SC sphere, along the  $z$  axis can be obtained from the radial component of the magnetic field. In order to compare them with the numerical simulations below, we now convert the magnetic field back to Cartesian coordinates and obtain,

$$\vec{B}_m^\pm(z) = \pm \hat{k} \frac{\mu_0 m}{4\pi} \sum_{n=0}^{\infty} n(n+1) (\pm z)^{(n-1)} P_n(\pm 1) \left[ \left( \frac{1}{d_+} \right)^{n+2} + \left( -\frac{1}{d_-} \right)^{n+2} \right], \quad (23)$$

where now  $+$  and  $-$  in  $\pm$  correspond to respectively positive and negative values for the  $z$  axis and  $\hat{k}$  is the unit vector along the  $z$  axis. Similarly, we find for the induced magnetic field by the SC sphere, with radius  $\gamma$  one has,

$$\vec{B}_{\text{SC}}^{\pm}(z) = \mp \hat{k} \frac{\mu_0 m}{4\pi} \sum_{n=0}^{\infty} n(n+1) \frac{\gamma^{(2n+1)}}{(\pm z)^{(n+2)}} P_n(\pm 1) \left[ \left( \frac{1}{d_+} \right)^{n+2} + \left( -\frac{1}{d_-} \right)^{n+2} \right]. \quad (24)$$

From equations (23) and (24) we obtain,

$$\vec{B}_m(z) = \vec{B}_m^{\pm}(z) = -\hat{k} \frac{\mu_0 m}{2\pi} \left[ \frac{1}{(z - d_+)^3} + \frac{1}{(z + d_-)^3} \right], \quad (25)$$

$$\vec{B}_{\text{SC}}^+(z) = -\vec{B}_{\text{SC}}^-(z) = \hat{k} \frac{\mu_0 m}{2\pi} \gamma^3 \left[ \frac{1}{(\gamma^2 - z d_+)^3} + \frac{1}{(\gamma^2 + z d_-)^3} \right]. \quad (26)$$

Then the net magnetic field along the  $z$  axis between the two dipoles with the SC sphere is given by the piecewise function:

$$\vec{B}_T(z) = \begin{cases} \vec{B}_m(z) + \vec{B}_{\text{SC}}^+(z) & z > \gamma, \\ 0 & -\gamma \leq z \leq \gamma, \\ \vec{B}_m(z) + \vec{B}_{\text{SC}}^-(z) & z < -\gamma. \end{cases} \quad (27)$$

Without the SC sphere present between the two dipoles,  $\vec{B}_T(z) = \vec{B}_m(z)$ .

We compute the  $z$  component of the force on the SC sphere and from the dipoles as,

$$\vec{F}_{\text{SC}}(d_+, d_-) = -\hat{k} \frac{\partial}{\partial z} \left( \vec{m} \cdot \vec{B}_{\text{SC}}^+(z) \right) \Big|_{z=d_+} + \hat{k} \frac{\partial}{\partial z} \left( \vec{m} \cdot \vec{B}_{\text{SC}}^-(z) \right) \Big|_{z=d_-}, \quad (28)$$

The final form of  $\vec{F}_{\text{SC}}$  is given by:

$$\vec{F}_{\text{SC}} = \hat{k} \frac{3}{2} \frac{\mu_0 m^2}{2\pi} \gamma^3 \left[ \frac{2d_-}{(\gamma^2 - d_-^2)^4} - \frac{2d_+}{(\gamma^2 - d_+^2)^4} + \frac{d_-}{(\gamma^2 + d_+ d_-)^4} - \frac{d_+}{(\gamma^2 + d_+ d_-)^4} \right]. \quad (29)$$

The properties of the trap can be explored by introducing displacements to the SC sphere. For this, we consider two parameters the total gap between the centers of two magnets,  $d = d_+ + d_-$  and the displacement  $2\delta = d_- - d_+$ . Then with the transformation  $d_{\mp} = (d/2) \pm \delta$ , we can write the  $\vec{F}_{\text{SC}}$  as a function of  $\delta$ . We do a series expansion of such a function and from this series that consists only of odd terms we approximately neglect all the higher order terms assuming small displacements, but the first order term. The resultant  $\vec{F}_{\text{SC}}(\delta)$  can be written as,

$$\vec{F}_{\text{SC}}(\delta) \sim -\hat{k} 384 \frac{\mu_0 m^2}{\pi} \gamma^3 \left[ \frac{14d^2 + 8\gamma^2}{(d^2 - 4\gamma^2)^5} - \frac{1}{(d^2 + 4\gamma^2)^4} \right] \delta. \quad (30)$$

For the separation between dipoles is much greater than the diameter of the SC sphere,  $d \gg 2\gamma$ ,  $\vec{F}_{\text{SC}}(\delta)$  becomes,

$$\vec{F}_{\text{SC}}(\delta) \sim -\hat{k} 4992 \frac{\mu_0 m^2}{\pi} \frac{\gamma^3}{d^8} \delta. \quad (31)$$

The magnitude of force in (31) is of the form of  $F_{\text{SC}}(\delta) = -k_z \delta$ , where  $k_z = 4992 \mu_0 m^2 \gamma^3 / (\pi d^8)$  is the spring constant or stiffness of the trap. It is also the negative slope of the force-displacement curve that can be drawn from equation (31). The gravitational pull also puts an extra force on the SC sphere and displaces it from the origin along the negative  $z$ -axis. Then the total force on the SC sphere along the  $z$ -axis becomes,  $-\hat{k}(k_z \delta + m_{\text{SC}} g)$ , where  $m_{\text{SC}}$  and  $g$  are the mass of the SC sphere and acceleration due to gravity. As a result, we can write the equilibrium position as,  $\delta_{\text{eq}} \sim -m_{\text{SC}} g / k_z$ . If the slope of the force-displacement curve is not going to vary from the origin to the equilibrium position and also approximates the trap as a harmonic one, the angular frequency in radian of the trap along the  $z$  axis at  $\delta_{\text{eq}}$  is given as  $\omega_z = \sqrt{k_z / m_{\text{SC}}}$ .

In order to understand how much the back action of the SC sphere affected the dipole magnetic field and the force due to it, we treat the presence of the SC sphere in the magnetic field as a perturbation and do not consider any back action from the SC sphere on the magnetic fields. To identify this case from the previous case we denote the force, stiffness, equilibrium position, and trap frequency, with an over-line above the corresponding symbols.

The force on the particle along the z-axis is then [16, 17],

$$\vec{F}_{SC} = \hat{k} \frac{\chi V}{\mu_0} B \frac{\partial B}{\partial z}, \quad (32)$$

where  $B = \sqrt{B_x^2 + B_y^2 + B_z^2}$ , with  $B_{x/y/z}$  is the x/y/z component of the magnetic field. Since we are considering a perfect superconductor we can consider  $\chi \sim -1$ . In contrast to the previous case, we consider  $d_+ = d_-$ . In order to obtain  $B_{x/y/z}$ , we write down  $\Phi_m$  directly in Cartesian coordinates from equation 13 as.

$$\Phi_m(x, y, z) = \frac{m}{4\pi} \left( \frac{(z - (d/2))}{(x^2 + y^2 + (z - (d/2))^2)^{3/2}} - \frac{(z + (d/2))}{(x^2 + y^2 + (z + (d/2))^2)^{3/2}} \right). \quad (33)$$

Then we can write  $B_x = -\mu_0 \partial \Phi_m(x, 0, 0) / \partial x$ ,  $B_y = -\mu_0 \partial \Phi_m(0, y, 0) / \partial y$ , and  $B_z = -\mu_0 \partial \Phi_m(0, 0, z) / \partial z$ . The  $B_z$  is same as in equation (25), as  $d_+ = d_- = d/2$

Since we are interested in the force along the z-axis alone, where  $x = y = 0$ ,

$$\vec{F}_{SC}(z) = -\hat{k} \frac{V}{\mu_0} B_m(z) \frac{\partial B_m(z)}{\partial z}, \quad (34)$$

Then from equation 30 using series expansion and considering only the first order we get,

$$\vec{F}_{SC} \sim -\hat{k} 3072 \frac{\mu_0 m^2}{\pi} \frac{\gamma^3}{d^8} \delta. \quad (35)$$

Comparing equation 31 and 35, we can see that the trap stiffness  $k_z \sim 1.625 \bar{k}_z$ , the equilibrium position  $\delta_{eq} \sim \bar{\delta}_{eq} / 1.625$ , and the trap frequency  $\omega_z \sim 1.27 \bar{\omega}_z$ .

To validate this analytical method, we also built a COMSOL model with the same geometry as that in the above analysis (Figure 4), except for magnet spheres instead of magnetic dipoles. The magnetic field of a magnet sphere with flux density  $B_{magnet}$  and volume  $V_{magnet}$  is identical to that of a magnetic dipole with moment  $m = \frac{1}{\mu_0} B_{magnet} V_{magnet}$ , so that would not affect the result. In the model, we took the SC sphere radius  $\gamma = 100 \mu m$ , magnet spheres radius  $R_{magnet} = 1000 \mu m$ , the distance between two magnets  $d = 4000 \mu m$ , magnet flux density  $B_{magnet} = 1 T$ . In the COMSOL simulation, the backaction of the superconductor to the magnetic field used to trap it is well considered. We get the vertical trap stiffness  $k_{z,COMSOL} = 0.32 N/m$ , which agrees well with  $k_z = 0.34 N/m$  from the above backaction effect involved analytical method using the same parameters. Considering  $k_z \sim 1.625 \bar{k}_z$ , we can then conclude that the backaction effect of a superconductor in a trapping magnetic field is significant and it would change the vertical trap stiffness by 62.5% in this case.

### C. FEM simulation in COMSOL

We simulate the levitation of superconducting flux qubit using the spherical micro-magnet in a 2D axisymmetric model using the commercial finite element method (FEM) package COMSOL. In this FEM model, we consider the flux qubit as a superconducting ring with the ideal Meissner effect. We find that the London penetration has a negligible effect on the results due to the large size of the flux qubit. Furthermore, by performing a fully 3D FEM COMSOL simulation we have determined that the levitated flux qubit is stable both vertically and horizontally, due to the loop shape of the flux qubit. We observe that the magnetic forces and torques will work to restore the qubit's equilibrium position and orientation when flux qubit horizontally shifts or tilts slightly. Thus the trapped flux qubit experiences complete rigid-body trapping.

To test the horizontal stability of the trapped flux qubit, we built a full 3D COMSOL model. In this model, we calculated the x component magnetic force ( $F_x$ ) at the condition of horizontal displacement ( $x$ ). We found that the magnetic force would be a restoring force when the flux qubit slightly shifts away from the balance position in the horizontal direction. Also, the torque on the flux qubit will restore it to the original position at the condition of tilting. It's also certain that the levitated flux qubit will be unstable when the horizontal displacement (or tilting) is too large. We have also calculated the horizontal trap frequency as around 19 Hz, and the tilting frequency as 9 Hz.



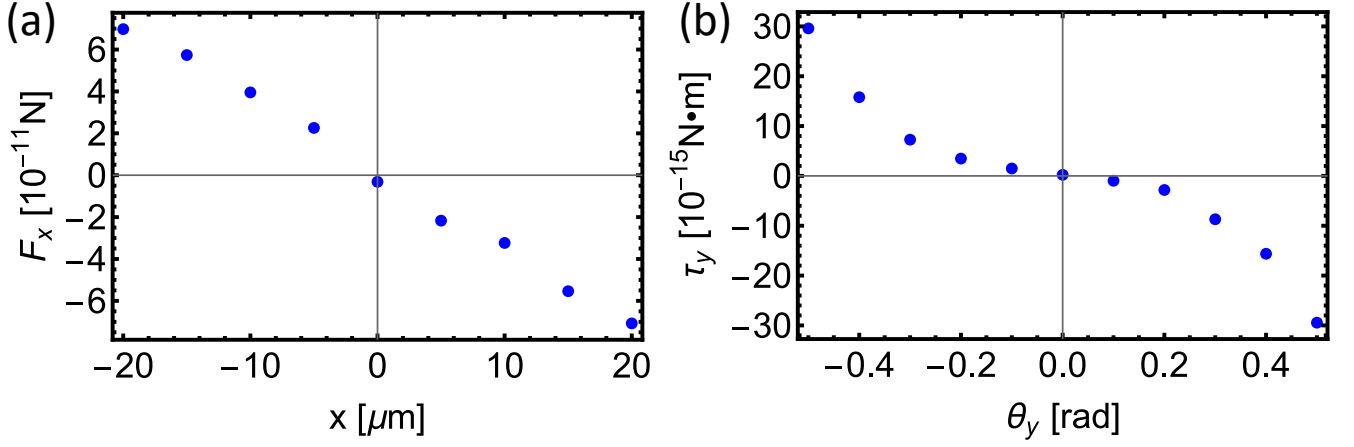


FIG. 5. The horizontal stability of the levitated superconducting flux qubit. (a) The magnetic force  $x$  component  $F_x$  as a function of the  $x$  direction horizontal displacement of the trapped flux qubit. (b) The torque  $y$  component  $\tau_y$  as a function of the tilting angle around  $y$ . The data was numerically calculated in a full 3D COMSOL model with flux qubit radius  $R = 183 \mu\text{m}$ .

TABLE I. System parameters and the values used to introduce the first method

Quantity	Symbol	Value	Unit
Density of YIG [18]	$\rho$	5110	$\text{kg}/\text{m}^3$
Remnant magnetic field of YIG [19]	$B_r$	$14.32 \times 10^{-3}$	T
Magnitude of persistent current in SC flux qubit	$I$	1000	nA
Mass of the Helium gas molecule	$M_g$	$6.65 \times 10^{-27}$	kg
Pressure of the gas surrounding the oscillator	$P_g$	$10^{-6}$	$\text{kg}/(\text{m s}^2)$
Boltzmann constant	$k_B$	$1.38 \times 10^{-23}$	$\text{m}^2/\text{kg}/(\text{K s}^2)$

TABLE II. System parameters and the values used to introduce the second method

Quantity	Symbol	Value	Unit
Radius of magnet sphere	$a$	12	$\mu\text{m}$
Radius of SC flux qubit	$R$	180 – 183.4	$\mu\text{m}$
Radius of cross-section of SC flux qubit	$r$	5	$\mu\text{m}$
Magnetic moment of magnet sphere	$m_{mag}$	$6.912 \times 10^{-9}$	$\text{A} \cdot \text{m}^2$
Remanent flux density of magnet sphere	$B_z$	1.2	T
Mass of SC flux qubit	$M$	$(2.41 - 2.45) \times 10^{-10}$	kg
Self inductance of SC flux qubit	$L$	$(8.28 - 8.48) \times 10^{-10}$	H
Vacuum magnetic permeability	$\mu_0$	$4\pi \times 10^{-7}$	H/m
Magnetic flux quantum	$\Phi_0$	$2.068 \times 10^{-15}$	Wb
Superposition current in SC flux qubit	$I$	$\pm 1000$	nA
Magnetic moment due to superposition current	$M_{sc}$	$(1.02 - 1.06) \times 10^{-13}$	$\text{A} \cdot \text{m}^2$
Equilibrium position of SC flux qubit	$h$	70 – 93	$\mu\text{m}$
Vertical trap frequency	$v_z$	10 – 43	Hz
Superposition states separation	$\Delta z$	7 – 100	nm
Zero point motion amplitude	$\delta z_{zpm}$	$6 \times 10^{-14}$	m
Superposition separation in terms of $\delta z_{zpm}$	$\chi$	$2 \times 10^6$	NA

#### IV. TABLE OF VARIABLES AND THEIR VALUES CONSIDERED IN THE PRESENT STUDY

- 
- [1] T. Wang, S. Lourette, S. R. O'Kelley, M. Kayci, Y. Band, D. F. J. Kimball, A. O. Sushkov, and D. Budker, Dynamics of a Ferromagnetic Particle Levitated over a Superconductor, *Physical Review Applied* **11**, 044041 (2019).
  - [2] B. De Lima Bernardo, F. Moraes, and A. Rosas, Drag force experienced by a body moving through a rarefied gas, *Chinese Journal of Physics* **51**, 189 (2013).
  - [3] J. Gieseler, A. Kabcenell, E. Rosenfeld, J. D. Schaefer, A. Safira, M. J. Schuetz, C. Gonzalez-Ballester, C. C. Rusconi, O. Romero-Isart, and M. D. Lukin, Single-Spin Magnetomechanics with Levitated Micromagnets, *Physical Review Letters* **124**, 163604 (2020).
  - [4] A. Vinante, A. Vinante, P. Falferi, G. Gasbarri, A. Setter, C. Timberlake, and H. Ulbricht, Ultralow mechanical damping with meissner-levitated ferromagnetic microparticles, *Physical Review Applied* **13**, 1 (2020).
  - [5] C. Timberlake, G. Gasbarri, A. Vinante, A. Setter, and H. Ulbricht, Acceleration sensing with magnetically levitated oscillators above a superconductor, *Applied Physics Letters* **115** (2019).
  - [6] J. Gieseler, B. Deutsch, R. Quidant, and L. Novotny, Subkelvin Parametric Feedback Cooling of a Laser-Trapped Nanoparticle, *Physical Review Letters* **109**, 103603 (2012).
  - [7] O. Chubar, P. Elleaume, and J. Chavanne, A three-dimensional magnetostatics computer code for insertion devices, *Journal of Synchrotron Radiation* **5**, 481 (1998).
  - [8] C. Navau, S. Minniberger, M. Trupke, and A. Sanchez, Levitation of superconducting microrings for quantum magnetomechanics, *Physical Review B* **103**, 174436 (2021).
  - [9] B. F. Edwards, D. M. Riffe, J.-Y. Ji, and W. A. Booth, Interactions between uniformly magnetized spheres, *American Journal of Physics* **85**, 130 (2017).
  - [10] O. Romero-Isart, L. Clemente, C. Navau, A. Sanchez, and J. I. Cirac, Quantum magnetomechanics with levitating superconducting microspheres, *Physical Review Letters* **109**, 147205 (2012).
  - [11] J. Hofer and M. Aspelmeyer, Analytic solutions to the Maxwell–London equations and levitation force for a superconducting sphere in a quadrupole field, *Physica Scripta* **94**, 125508 (2019).
  - [12] M. W. Coffey, Levitation force between a point magnetic dipole and superconducting sphere, *Journal of Superconductivity and Novel Magnetism* **13**, 381 (2000).
  - [13] Q.-G. Lin, Analytic solutions to Maxwell–London equations and levitation force for a general magnetic source in the presence of a long type-II superconducting cylinder, *The European Physical Journal B* **54**, 27 (2006).
  - [14] J. L. Perez-Diaz and J. C. Garcia-Prada, Interpretation of the method of images in estimating superconducting levitation, *Physica C: Superconductivity and its Applications* **467**, 141 (2007).
  - [15] M. W. Coffey, London model for the levitation force between a horizontally oriented point magnetic dipole and superconducting sphere, *Physical Review B* **65**, 214524 (2002).
  - [16] M. C. O'Brien, S. Dunn, J. E. Downes, and J. Twamley, Magneto-mechanical trapping of micro-diamonds at low pressures, *Applied Physics Letters* **114**, 053103 (2019).
  - [17] J. P. Houlton, M. L. Chen, M. D. Brubaker, K. A. Bertness, and C. T. Rogers, Axisymmetric scalable magneto-gravitational trap for diamagnetic particle levitation, *Review of Scientific Instruments* **89**, 125107 (2018).
  - [18] T. Seberston, P. Ju, J. Ahn, J. Bang, T. Li, and F. Robicheaux, Simulation of sympathetic cooling an optically levitated magnetic nanoparticle via coupling to a cold atomic gas, *Journal of the Optical Society of America B* **37**, 3714 (2020).
  - [19] M. A. Musa, R. S. Azis, N. H. Osman, J. Hassan, and T. Zangina, Structural and magnetic properties of yttrium iron garnet (YIG) and yttrium aluminum iron garnet (YAIG) nanoferrite via sol-gel synthesis, *Results in Physics* **7**, 1135 (2017).